Journal of Bioenergetics and Biomembranes, Vol. 34, No. 6, December 2002 (© 2002)

Modeling the Transmembrane Arrangement of the Uncoupling Protein UCP1 and Topological Considerations of the Nucleotide-Binding Site

Amalia Ledesma,[1] Mario García de Lacoba,[1] Ignacio Arechaga,[2] and Eduardo Rial[1,3]

Received July 19, 2002; accepted October 10, 2002

The uncoupling protein from brown adipose tissue (UCP1) is a mitochondrial proton transporter whose activity is inhibited by purine nucleotides. UCP1, like the other members of the mitochondrial transporter superfamily, is an homodimer and each subunit contains six transmembrane segments. In an attempt to understand the structural elements that are important for nucleotide binding, a model for the transmembrane arrangement of UCP1 has been built by computational methods. Biochemical and sequence analysis considerations are taken as constraints. The main features of the model include the following: (i) the six transmembrane α-helices (TMHs) associate to form an antiparallel helix bundle; (ii) TMHs have an amphiphilic nature and thus the hydrophobic and variable residues face the lipid bilayer; (iii) matrix loops do not penetrate in the core of the bundle; and (iv) the polar core constitutes the translocation pathway. Photoaffinity labeling and mutagenesis studies have identified several UCP1 regions that interact with the nucleotide. We present a model where the nucleotide binds deep inside the bundle core. The purine ring interacts with the matrix loops while the polyphosphate chain is stabilized through interactions with essential Arg residues in the TMH and whose side chains face the core of the helix bundle.

KEY WORDS: Uncoupling protein; UCP1; AAC; nucleotide binding; mitochondria; molecular modeling.

The uncoupling proteins are members of a protein superfamily formed by the metabolite carriers of the mitochondrial inner membrane (reviewed in Aquila *et al*., 1987; Walker and Runswick, 1993). These mitochondrial transporters have a molecular mass of around 32 kDa and have a tripartite structure where a domain of around 100 amino acids is repeated three times. Each domain contains two transmembrane regions usually connected by word a long hydrophilic loop (Fig. 1). Since the functional carrier is a homodimer, this protein superfamily can be included in the vast group of secondary transporters that present a functional unit formed by 12 transmembrane segments (reviewed in Saier, 2000a,b).

The biological function of the uncoupling proteins is the dissipation of the proton electrochemical potential gradient generated by the respiratory chain. Genes coding for uncoupling proteins are widely distributed not only among animals but also among plants (Ricquier and Bouillaud, 2000). Their ubiquitous presence suggests that uncoupling may be a common strategy to regulate the efficiency of oxidative phosphorylation. This mechanism could serve several biological functions: thermogenesis, energy expenditure in situations where there is surplus, maintenance of the redox balance when excess of NAD(P)H is produced, or lowering the production of reactive oxygen species (reviewed in Boss *et al*., 2000; Stuart *et al*., 2001).

In mammals five members of this family have been described. UCP1 was the first uncoupling protein described. Therefore, it is the best-characterized. It is only present in brown adipose tissue and it clearly has a thermogenic role (reviewed in Nicholls and Locke, 1984). UCP2

Key to abbreviations: UCP, uncoupling protein; AAC, ADP/ATP carrier; PiC, phosphate carrier; SBCGP, single binding center gated pore; TMS, transmembrane segment; TMH, transmembrane α-helix.

[1]Centro de Investigaciones Biológicas, CSIC, Velázquez 144, 28006 Madrid, Spain.

[2]MRC-Dunn Human Nutrition Unit, Welcome/MRC Building, Cambridge, United Kingdom.

[3]To whom correspondence should be addressed; e-mail: rial@cib.csic.es.

0145-479X/02/1200-0473/0 © 2002 Plenum Publishing Corporation

Fig. 1. Alignment of the amino acid sequences of the uncoupling protein UCP1 and the adenine nucleotide translocator (AAC). UCP1 sequences are from hamster (M.a.) and rat (R.n.). AAC sequences correspond to isoform 1 from beef heart (B.t. AAC1) and isoform 2 from *S. cerevisiae* (S.c. AAC2). Boxes indicate the regions that in UCP1 correspond to the transmembrane helices (TMHs) used in the modeling. Residues that have been shown, by photoaffinity labeling, to interact with the nucleotide are double-underlined. The underlined region in S.c. AAC2 also interacts with the nucleotide although the specific amino acids involved are not known. Residues in bold are those identified by site-directed mutagenesis to be essential for nucleotide binding.

is ubiquitously present although its expression level varies among organs. UCP3 is only expressed in brown adipose tissue and skeletal muscle. Finally, UCP4 and BMCP1 are only present in brain (reviewed in Boss *et al*., 2000; Ricquier and Bouillaud, 2000; Stuart *et al*., 2001). The activity of the uncoupling proteins is subject to regulation at gene expression and mitochondrial level. Purine nucleotides and free fatty acids seem to affect the activity of all these proteins (Jaburek *et al.*, 1999; Klingenberg and Echtay, 2001), although these effects are controversial (Hagen *et al*., 2000; Rial *et al*., 1999) and their physiological significance remains to be defined.

The physiological regulation of UCP1 is well established (reviewed in Nicholls and Locke, 1984; Rial and González-Barroso, 2001). Purine nucleotides maintain the protein inhibited by binding to a site from the cytosolic side of the membrane. Noradrenaline signals the brown adipocyte the initiation of thermogenesis. Binding of noradrenaline to β-receptors leads to a lypolitic cascade that mobilizes the triglyceride stores. The fatty acids released serve two functions. They are the substrates for mitochondrial oxidation and activators of UCP1. Therefore, fatty acids override the nucleotide inhibition.

Obtaining high-resolution structural data of integral membrane proteins is still a major challenge. Thus, while some 15,000 structures of proteins have been solved at atomic resolution, less than 50 correspond to membrane proteins and around half of these are repeated structures (i.e. same proteins from different species or under different crystallization conditions). These results contrast with the proportion of ORFs that appear to encode membrane proteins, which is around 30%. Generation of models is a common strategy to rationalize the structural organization of proteins and aids the design of new experiments. Several approaches are generally combined to get an insight into the structure. These include sequence analysis, recollection of mutagenesis data, low resolution biophysical data, or homology modeling derived from templates.

In the present paper we intend to put together the data available from nucleotide-binding studies, structural information, site-directed mutagenesis, and sequence analysis to analyze the transmembrane arrangement of the uncoupling protein UCP1 and to model the binding site for purine nucleotides.

THE UNCOUPLING PROTEIN UCP1 AS A GATED PORE

Transport proteins are divided, according to their transport mechanism, into two categories: channels and carriers. Channels open for limited periods and during this time they allow the movement of several million molecules per second. Usually, the channel gate opens after binding

of a regulatory ligand. On the other hand, carriers present a mechanism that resembles the catalytic cycle of an enzyme. There is a substrate binding site whose access from either side of the membrane is controlled by gates. When the substrate reaches its binding site from one side of the membrane, the binding energy drives a conformational change that opens the gate in the opposite site of the membrane and substrate is released. Despite this apparent clear difference between transport modes, often the underlying mechanism of transport cannot be determined from kinetic data. Thus, a channel may approach the carrier kinetics if, for example, it goes through several conformational states (Hernández, 2001; Krämer, 1994; Läuger, 1987).

More strikingly, it has been shown that carriers can also display channel-like kinetics. Examples are the γ-aminobutyrate transporter GAT-1 that becomes a chloride channel (Cammack and Schwartz, 1996), the chloroplast triose phosphate/phosphate translocator that can transport Pi and chloride (Schwarz *et al*., 1994) or the Na^+/glucose transporter hSGLT1 that behaves like a H^+ channel (Quick *et al*., 2001). Several members of the mitochondrial carrier family have also been shown to display channel conductances. Thus, in the presence of Ca^{2+}, the ADP/ATP carrier (AAC) is converted into a bongkrekate-sensitive channel with a conductance that can go up to 600 pS (Brustovetsky and Klingenberg, 1996). The phosphate carrier (PiC) displays a conductance of around 40 pS, which that can be reversibly blocked by Pi (Herick *et al*., 1997). Finally, UCP1 has been shown to behave as a nucleotide-sensitive chloride channel with a unit conductance of 75 pS (Huang and Klingenberg, 1996).

Structural and sequence data suggest that channels and carriers probably have a common evolutionary origin that would be conserved in their basic catalytic principles (Saier, 2000a,b). It has been proposed that primitive channels have evolved into more complex systems such as the secondary carriers or the group translocators. The simplest transporters would be channel proteins formed by just two transmembrane segments (TMSs). Examples of this group would be the eukaryotic inward rectifier family or the prokaryotic potassium channel (KcsA) (Anderson and Greenberg, 2001). The vast majority of transporter families are formed by α-helical channel-type arrangements, and their functional unit generally consists of between 12 and 14 TMSs. Through evolution, these long polypeptide chains have been generated by gene duplication events (Anderson and Greenberg, 2001; Saier, 2000a,b). Thus, the mitochondrial transporter family evolved from a primordial 2-TMS encoding element that was triplicated, and the functional carrier protein is a homodimer. Similar evolutionary pathways have been described for most transporter families (Saier, 2000a,b). As we said earlier, these relationships suggest the need for the formation of a basic structure, probably a hydrophilic translocation pore, regardless of the specific transport mechanism involved (Arechaga *et al*., 2001; Krämer, 1994).

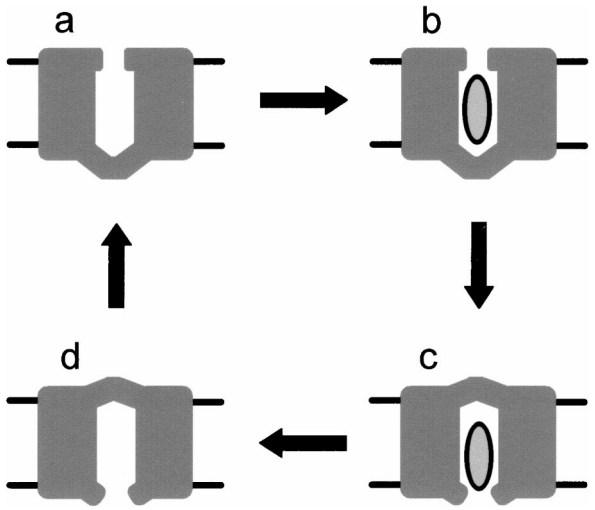

Fig. 2. Catalytic cycle of transporters according to the model "Single Binding Center Gated Pore" (SBCGP). Catalytic cycle starts with the unloaded carrier in which one of the gates that control the access to the substrate binding site is opened (a). Substrate binds to the carrier (b) and the substrate–protein interaction energy at the transition state drives a conformational rearrangement that leads to the translocation (c). Gate opens on the opposite side of the membrane and the substrate dissociates from a binding center (d). The unloaded carrier switches back through a new transition state to the original side of the membrane (a).

In 1991, Klingenberg rationalized the mechanism of transport for the ADP/ATP carrier (AAC) with a scheme named Single Binding Center Gated Pore (SBCGP) (Klingenberg, 1991) (Fig. 2). The key feature of the model is the existence of a substrate-binding center in the core of the protein whose access is controlled by gates. The substrate gains access to the center through one gate and binds to the protein, and the interaction energy drives the conformational change that leads to the closure of the entrance gate and the opening of the exit gate. This scheme can be generalized to most transport systems and the main difference between carriers and channels would lie in the accessiblility to the binding center. Thus, while in carriers the two gates must not be opened at any given time, in channels there either is only one gate or the two gates open simultaneously. The switch of a carrier to a channel mode can be understood if the modification of the carrier structure results in the concurrent opening of the two gates.

In line with these evolutionary considerations, functional data has also suggested that mitochondrial carriers

consist of two domains (Dierks *et al*., 1994). The core of the protein would correspond to the evolutionary conserved element and would constitute a channel-like domain, while the gating domain would confer the transporter its specific characteristics. Modification of the gating domain leads to dramatic changes in the transport properties. Thus, it has been demonstrated that chemical modification of sulfhydryl groups in several mitochondrial carriers alters markedly the substrate specificity (Dierks *et al*., 1990; Indivieri *et al*., 1992; Stappen and Krämer, 1993). For example, in the aspartate/glutamate carrier (AGC), the exchange of aspartate for glutamate is converted into a uniport with poor specificity. Substrates like sulfate, arginine, or glucose are transported by the modified protein (Dierks *et al*., 1990).

The location of the gates has been investigated in the AAC and UCP1. Terada and coworkers have demonstrated the involvement of the three matrix loops in the AAC that undergo important rearrangements during the catalytic cycle (Hashimoto *et al*., 1999; Majima *et al*., 1994, 1995). The sulfhydryl groups involved in the shift of the specifities have been identified in the AAC in the first and second matrix loops. Additionally, our work with UCP1 has pointed out the implication of the third matrix loop in the control of transport. Deletion of amino acids 261–269 results in the formation of a pore that allows the movement of solutes of at least 1000 Da (González-Barroso *et al*., 1999). The 3D structure of a peptide corresponding to this UCP1 region has been solved by NMR, and one of the most interesting features is that residues 263–268 form a short α-helix (González-Barroso *et al*., 1999). This helix is located at the N-terminal ends of the TMS6, and the link between the two helices is defined by the sequence Gly-Phe-Ala-Pro, a putative β-turn of type VIII. Similar sequences are present at the N-terminal ends of TMS2 and TMS4. Mutations in any of these three turns lead to major changes in the control of transport in UCP1, thus suggesting the implication of the three matrix loops in the control of transport (González-Barroso *et al*., 1997).

A transition from carrier to pore in mitochondrial transporters may be of physiological relevance. It has been proposed that the AAC is part of the permeability transition pore complex. Opening of the pore allows passage of molecules of up to 1500 Da and leads to mitochondrial swelling, release of cytochrome *c* and the subsequent apoptotic cascade (for reviews see Brown *et al*., 1999). In the late 80s, Crompton *et al*. (1988) demonstrated that the permeability transition could be inhibited by cyclosporin A. This drug is an inhibitor of cyclophilin A, a peptidyl–prolyl *cis–trans* isomerase. Halestrap *et al.* proposed subsequently that cyclophilin A could be binding to Pro^{61} and the isomerization could lead to the opening of the pore (Halestrap and Davidson, 1990). It has been recently described that thiol-cross-linking reagents, that open the pore and trigger apoptosis, may be reacting with Cys^{56} of the AAC (Costantini *et al*., 2000). This residue is in the vicinity of Pro^{61} and are both located in the first matrix loop. In line with these observations, it has been shown that cyclophilin D binding to the AAC prevents the dimerization of the carrier that is caused by cross-linking with copper-phenantroline of Cys^{56} of two AAC monomers (Halestrap *et al*., 2002). Finally, it is interesting to note that these Pro and Cys residues are not conserved in yeast isoforms of the AAC, and yeast mitochondria do not undergo a cyclosporin-sensitive permeability transition (Halestrap *et al*., 1997). Thus it could be envisaged that the conformational change at Pro^{61} leads to the opening of the gate and thus the carrier–pore conversion.

THE LOCATION OF THE NUCLEOTIDE-BINDING SITE IN THE AAC AND UCP1

The AAC and the UCPs are the only mitochondrial carriers that interact, under physiological conditions, with nucleotides. It has been reported that the PiC may also bind nucleotides since Pi transport is competitively inhibited by ATP (Stappen and Krämer, 1994) and analogs of fluoresceine (whose structure resembles that of a purine nucleotide) bind to the carrier (Majima *et al*., 2001). These mitochondrial transporters do not catalyze the hydrolysis/formation of the phosphate–phosphate bonds. Therefore, Mg^{2+} does not participate in the binding and the consensus motifs present in ATPs-hydrolyzing/synthesizing enzymes (Walker *et al.*, 1982) are absent. However, AAC and UCP1 present some characteristics similar to other nucleotide-binding proteins. Thus, thermodynamic studies have demonstrated that nucleotide binding to UCP1 results in a small enthalpy increase while the entropy change is large (Huang and Klingenberg, 1995). This is a common feature in a nucleotide's binding to proteins (Ross and Subramanian, 1981). The large entropy change, which drives the binding, has been interpreted as a result of the removal of water molecules from the binding site and the establishment of strong hydrophobic and ionic interactions (Huang and Klingenberg, 1995). The elucidation of the 3D structure of enzymes where the adenine nucleotides are bound has revealed that they bind in the *anti* conformation. Examples are the ATP bound in actin (Kabsch *et al*., 1990), adenylate kinase (Fry *et al*., 1986), or the mitochondrial F_1-ATPase (Abrahams *et al*., 1994). NMR investigation of ATP binding to the AAC has shown that the bound nucleotide is also in the *anti* conformation

(Huber *et al*., 1999). We will now summarize the data available on the binding site in UCP1 and AAC.

The Binding Pocket for the Purine Ring and the Ribose Moiety

First data on the possible location of the nucleotide-binding site in AAC and UCP1 have come from photoaffinity labeling experiments. The nucleotide derivatives used in these experiments possess a reactive group in the purine ring or linked to the ribose. Dalbon *et al.* (1988) used 2-azido-ADP with the bovine heart AAC and found the label predominantly in two regions: Lys^{162}, Lys^{165}, and Ile^{183} of the second AAC repeat and Val^{254} and Lys^{259} in the third matrix loop. Mayinger *et al.* (1989) used 2-azido- and 8-azido-ATP to label the yeast isoform AAC2. With the two derivatives the label was incorporated to a region between residues 172 and 210 that would correspond mainly to the fourth transmembrane segment. Finally, the ADP analog 2-azido-3′-*O*-naphthoyl-ADP has recently been used to identify the binding regions in the yeast AAC (Dianoux *et al*., 2000). Two fragments were labeled: in the second matrix loop a segment delimited by residues 183–191 and in the C-terminal region the peptide-containing residues 311–318. Fluoresceine derivatives are structurally related to adenine nucleotides; hence they have often been used as probes for nucleotide-binding proteins. Majima *et al.* (1993) found that the fluoresceine derivative eosin-5-maleimide (EMA) reacted with cysteines 56, 159, and 256, each located on the central portion of a different matrix loop. However, EMA preferentially labels Cys^{159} to inhibit ADP transport. The labeling occurs from the matrix side of the protein and it is prevented by bongkrekic acid, ADP, or palmitoyl-CoA (Majima *et al*., 1994). Interestingly, carboxyatractylate also prevented EMA labeling and this inhibitor binds to the AAC from the cytosolic side of the membrane. All these data have been interpreted as evidence for the role of matrix loops in the gating of the carrier and that conformational changes in these loops regulate its transport activity (Majima *et al*., 1994). It has also been suggested that the hydrophobic residues that are in the vicinity of Cys^{159} (Phe^{153}, Leu^{156}, Ile^{160}, Ile^{163}, and Phe^{164}) could form a hydrophobic pocket that would bind the A/B rings from eosin Y that resemble the adenine moiety in ADP (Majima *et al*., 1998).

The nucleotide-binding site in UCP1 has also been investigated by photoaffinity labeling. However, before comparing the experimental data there are a number of fundamental differences between these two related carriers that should be remembered. First, UCP1 binds nucleotides from the cytosolic side of the protein while in AAC nucleotides interact from both sides of the membrane. Second, nucleotides are transport substrates for the AAC whereas in UCP1 they bind to inhibit the transport activity. As it has been previously discussed (Arechaga *et al*., 2001; Klingenberg, 1991), this latter difference would be the basis for the apparent discrepancies in the binding affinities and specificities. Thus, the high specificity in AAC is indicative of the need of a closer protein–nucleotide interaction, because the binding energy has to drive the translocation. Binding leads to the change in the conformation of the binding center to a lower affinity, facilitating nucleotide release. The apparent higher affinity but lower specificity of UCP1 reflects, in turn, the fact that the nucleotide is just an inhibitor and its binding should only lead to a minor conformational rearrangement.

Photoaffinity labeling experiments of hamster UCP1 have been performed with three different ATP derivatives, 8-azido-ATP, 2-azido-ATP, and 3′-*O*-(5-fluoro-2,4-dinitrophenyl) adenosine-5′-triphosphate (FDNP-ATP). The three labeled residues in the third matrix loop (Mayinger and Klingenberg, 1992; Winkler and Klingenberg, 1992). 8-Azido-ATP probably reacted with Thr^{259} while 2-azido-ATP labeled Thr^{264}. FDNP-ATP was probably bound to Cys^{253}. This was deduced from the ability of tetranitromethane to prevent the FDNP-ATP incorporation and the previous finding that tetranitromethane, by modifying a cysteine residue, inhibits nucleotide binding (Rial and Nicholls, 1986). This singular involvement of the third loop in nucleotide binding should not be taken as an indication of the lack of a role of the other two matrix loops. In fact, deletion of a conserved glycine in any of the three loops (Gly^{76}, Gly^{175}, and Gly^{269}) has profound effects on the nucleotide regulation of UCP1 (González-Barroso *et al*., 1999).

The nucleotide specificity should also provide valuable information on the structure of the binding centre. As we just said, it is noteworthy that the AAC presents a high specificity towards the substrates and it seems that the recognition of the adenine moiety is of fundamental importance. Thus, ADP and ATP are transported while GDP or GTP are excluded. The ability of the AAC to bind the nucleotide analog eosin Y and the exclusion of guanine nucleotides has been rationalized in terms of the differences in the electrostatic potentials of the adenine or the A/B ring of eosin compared with that of the guanine ring (absence of a negative potential at N1) (Majima *et al*., 1998) (Fig. 3). It should be noted, however, that eosin Y is not translocated and inhibits ADP transport (Majima *et al*., 1998). In contrast, bulky substituents bound to positions 2′- or 3′-*O*- of the ribose are well tolerated. Clear examples are the dansyl derivatives that are not only bound but also transported under energized conditions. It is particularly striking that the derivative DAN-AMP is efficiently

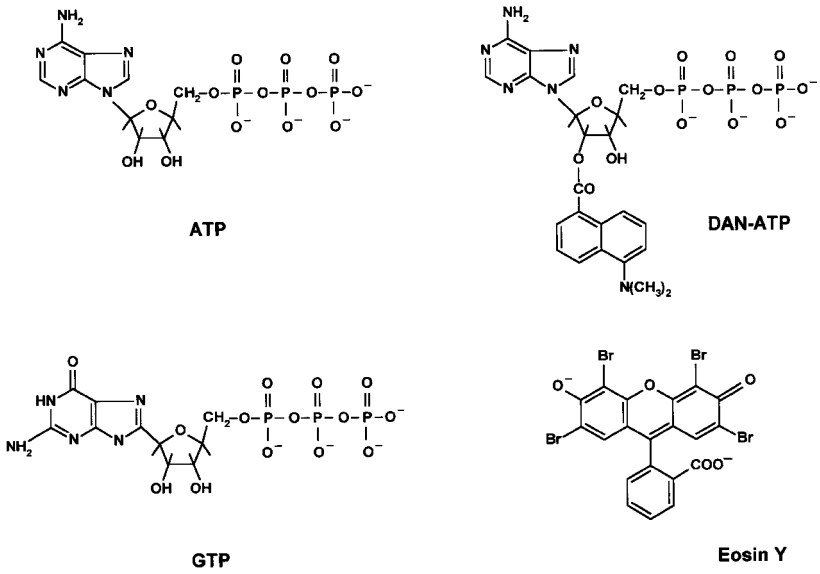

Fig. 3. Chemical formula of purine nucleotides and nucleotide analogs used in binding assays with the AAC and UCP1.

taken up by energized rat liver mitochondria (Klingenberg *et al*., 1984).

The earliest experiments revealed that the uncoupling protein UCP1 presents a much broader specificity since any purine nucleoside di- or triphosphate binds to the protein and inhibits its proton conductance. Monophosphate purine nucleotides or any pyridine nucleotides are not accepted (Heaton and Nicholls, 1977). Small substitutions in the purine ring are well tolerated and indeed the analogs 2-azido-, 8-azido-, or 8-bromo-ATP do bind and inhibit UCP1. In fact, identification of the uncoupling protein UCP1 as a 32-kDa protein was achieved by affinity labeling with 8-azido-ATP (Heaton *et al*., 1978). Like in the AAC, bulkier substituents are acceptable if introduced in the 2′- or 3′-*O*- position of the ribose moiety. Thus, FDNP-ATP has been successfully used for photoaffinity labeling (Mayinger and Klingenberg, 1992) and dansylated purine nucleotides—where a (5-dimethylamino)-naphthalene residue is linked to the ribose (Fig. 3)—bind to UCP1 with affinities that are even higher than the natural ligands (Huang and Klingenberg, 1995). Differences in the behavior of UCP1 and AAC with respect to these nucleotides are also remarkable. Thus while DAN-AMP is translocated by the AAC, this monophosphate derivative does not bind to UCP1 (Huang and Klingenberg, 1995).

The structure of the binding pocket for the purine ring in other nucleotide-binding proteins does not present a uniform pattern. Rossman *et al.* (1975) observed that in most dehydrogenases there exists a hydrophobic groove that accommodates the adenosine moiety of NADH. For example, it is remarkable how in the glyceraldehyde-3-phosphate dehydrogenase, the adenine ring is sandwiched between two Phe residues (Rossman *et al.*, 1975). A similar situation is found in the mitochondrial F_1-ATPase. In the catalytic β subunit, the purine ring is between Phe^{424} and Tyr^{345}. A third aromatic residue (Phe^{418}) also contributes to the formation of the hydrophobic pocket (Abrahams *et al*., 1994; Menz *et al*., 2001). In contrast, in the superfamily of the regulatory GTP hydrolases (G proteins), stabilization of the bound nucleotide is achieved through the formation of specific hydrogen bonds to the guanine ring (Sprang, 1997). This protein family presents two conserved sequence regions responsible for recognition of the guanine ring: NKxD and (T/G)(C/S)A. The first and last residues of the NKxD sequence specifically hydrogen-bond to the guanine ring while the methylene groups of the Lys side chain provide a hydrophobic surface that lies over the purine ring. Stabilization on the opposite side of the ring shows significant variations among the family members. The adenylate kinase from *E. coli* presents, in the ATP-binding site, a pocket for the adenine moiety formed between Arg^{119} and the peptide backbone from Pro^{201} to Val^{202}. There is only one hydrogen bond, which is formed between the N6 of the adenine and the carbonyl oxygen of a Lys residue (Berry *et al*., 1994). As a final example of the diversity in the formation of the pocket to accommodate the purine ring we will mention the kinesin family. The kinesins also present a conserved element (RxRP) that forms stacking interactions with the adenosine ring. The

methylene groups of the Arg plus those from the Pro residue are found on one side of the ring while on the other side the imidazole ring of a His residue provides a hydrophobic surface (Sack *et al*., 1999).

Binding of the Polyphosphate Chain

The Mg^{2+} ion participates in the binding of nucleotides in nearly all enzymes where there is ATP synthesis or hydrolysis. These enzymes present a highly conserved sequence termed the phosphate-binding loop (P loop or Walker A motive) [GXXXXGLT] (Walker *et al*., 1982). In the mitochondrial F_1-ATPase, for example, Mg^{2+} is coordinated to the oxygen atoms of the β- and γ-phosphates and probably also to the hydroxyl group of the Thr in the P loop (Abrahams *et al*., 1994). As we have already mentioned, this metal ion does not participate in the binding of the nucleotides to AAC or UCP1, and therefore it is not surprising that the P-loop sequence is absent.

Early studies on nucleotide binding to UCP1 showed that it was highly pH dependent (Nicholls, 1976). This property has been thoroughly studied subsequently and has pointed out to the implication of at least two protonable groups in the binding of the nucleotide (Klingenberg, 1988) that were later identified as Glu^{190} and His^{214} (Echtay *et al*., 1998; Winkler *et al*., 1997). The two residues are located on the cytosolic side of the protein. Glu^{190} displays a pK_a around 4 and it has been proposed that its protonation opens the access to the binding site. The second residue displays a pK_a of 7.2 and it has been proposed that it will only affect the binding of triphosphate nucleosides, so that if protonation of His^{214} does not take place the binding of the triphosphate species will not happen and the reaction will slowly result in a tight binding of the nucleotide diphosphate. Site-directed mutagenesis studies have also suggested the involvement in binding of phosphates of several intrahelical Arg residues. Mutation of either Arg^{83}, Arg^{182}, or Arg^{276} leads to the loss of the binding capacity at physiological pH. In contrast, mutation of Arg^{91} leads to minor changes in the binding affinity (Echtay *et al*., 2001; Modriansky *et al*., 1997). It is interesting to note that all these residues (Glu^{190}, His^{214}, Arg^{83}, Arg^{182}, and Arg^{276}) are strictly conserved among the UCPs. Photoaffinity labeling signified the implication of the C-terminal end of the third matrix loop in the binding. Since Lys^{268} is located close to the labeling site, it could interact with the nucleotide but this posibility has been ruled out by site-directed mutagenesis (González-Barroso *et al*., 1999; Modriansky *et al*., 1997). Similarly, mutation of Lys^{72} located in the first matrix loop does not modify the binding parameters (Modriansky *et al*., 1997).

Apart from the above-mentioned Glu^{190}, there are other acidic residues that when mutated affect the binding of the nucleotides. Asp^{27} is another intrahelical conserved residue and it is located in TMS1 at a similar depth as the Arg residues 83, 182, and 276. The mutants Asp27Glu or Asp27Asn show a marked decrease in the binding affinity. It has been proposed that the residue does not participate directly in the binding center but it may form an ionic bond with one of the intrahelical Arg residues and contribute to the protein stability (Echtay *et al*., 2000). Finally, the acidic pair formed by residues Asp^{209} and Asp^{210} seem to affect the binding of the nucleotide through their influence on His^{214}.

Site-directed mutagenesis of the AAC has identified a large number of residues as essential for carrier function. However, as we said in the previous section, setting differences and analogies between AAC and UCP1 in the binding of nucleotides finds several obstacles. Probably the most noticeable are, first, the presence in the AAC of binding sites on both sides of the membrane and second the need for a translocation event. This fact is exemplified with the differences in the amino acid sequence (Fig. 1). Thus, most of the conserved residues that have been found important for nucleotide binding in UCP1 are not present in AAC: Asp^{27} is replaced by Lys, Arg^{182} by Gly, Glu^{190} by Tyr residue, and His^{214} by Trp or Phe. Finally, the pair Asp^{209} and Asp^{210} is replaced by His-Ile in mammals and Ser-Phe in the three yeast isoforms. Arg^{83} is, however, present in the AAC (Arg^{96} in the yeast AAC2) and has been shown to be important for the carrier activity (see below). This residue is not conserved in other members of the mitochondrial carrier family.

The search of the literature for mutagenesis data that pinpoint residues involved in the nucleotide binding to the AAC finds a methodological barrier. Experiments designed to characterize AAC mutants rely on the discrimination of a competent carrier. An inactive carrier may arise from incorrect folding, loss of critical residues in the binding centers, or restraining the protein reorganization that leads to substrate translocation. Therefore, establishing which residues are only involved in the interaction of the nucleotide with the protein is not possible. There are, obviously, many charged residues involved in the carrier activity and some of them are characteristic of the AAC family. We will only present here the more prominent ones. Those residues have been shown to have a critical role in transport in the yeast isoform AAC2.

In the AAC family there are three intrahelical Arg residues that are well conserved. Arg^{96} and Arg^{204} have been found to be essential for carrier function while Arg^{294} has not been (Müller *et al*., 1996; Nelson *et al*., 1993). However, Arg^{294} seems to have a fairly relevant

role. First, it is highly conserved across the mitochondrial carrier family. Second, replacement of this residue by Ala results in a mutant AAC2 that catalyzes a normal ADP/ADP exchange while the ATP/ATP exchange is drastically reduced. Furthermore, it can exchange $ADP_{external}$ for $ATP_{internal}$ at rates comparable to the wild-type protein while the $ATP_{external}/ADP_{internal}$ activity is nearly abolished. These results have been interpreted as being indicative of an increase in the K_m for the external ATP while the K_m for the external ADP or the internal ATP remain unaffected (Heidkämper *et al*., 1996). It has been speculated that this Arg residue could interact transiently with the negative charges on the substrate during transport (Nelson *et al*., 1998). On the other hand, the Arg294Ala mutation can be reverted by removing the negative charge of Glu^{45}, which would argue against a direct involvement in the binding of the additional ATP charge.

In the third matrix loop there exists an Arg triplet (252–254) that is a distinctive feature of the AAC family and the three residues are also critical for carrier function (Müller *et al*., 1996; Nelson *et al*., 1993). Curiously, search for supressor mutations that compensate for mutations in the Arg triplet revealed that 14 out of 15 revertants appeared on a narrow ring-like plane on the opposite face of the protein, i.e. close to the cytosolic side of the membrane (Nelson and Douglas, 1993). Another critical residue is Lys^{38} in TMS1, which is also characteristic of the AACs and, as we said earlier, in the homologous position in the UCPs there is an Asp. Several of these residues have been proposed to participate in salt bridges. Thus, analysis of supressor mutations have suggested that Lys^{38} could make a charge-pair with Glu^{45}. Since Glu residue has also been shown to interact with Arg^{294} (see above), it would imply that there could be switching of charge-pairs during transport (Nelson *et al*., 1998). Asp^{149}, which is at equivalent position to Glu^{45} at the beginning of the second matrix loop, could also be forming salt bridges with Arg^{252} and with Arg^{152}, thus again reemphasizing a possible dynamic nature of these interactions. Since most of these charges ($AAC2_{yeast}/UCP1_{hamster}$: Glu^{45}/Asp^{34}, Asp^{149}/Glu^{134}, Arg^{152}/Lys^{137}, Arg^{252}/Lys^{236}, Arg^{294}/Arg^{276}) are highly conserved in the mitochondrial carrier family, it suggests that these charge-pairs could be of fundamental importance for the functioning of these transporters (Nelson *et al*., 1998).

MODEL BUILDING FOR THE TRANSMEMBRANE ARRANGEMENT OF THE UCP1

The growing number of amino acid sequences of membrane proteins and the difficulty in obtaining high-resolution structures have resulted in an increasing effort to develop methods of structure prediction (for reviews see Simon *et al*., 2001, and references therein). The available bioinformatic tools have made the prediction of membrane-spanning regions nearly an elementary task, but modeling the packing of these transmembrane segments is still a difficult assignment. Nevertheless, the membrane environment imposes important restrictions on the number of possible folds, and therefore tertiary structure predictions are easier to make than those for globular proteins. To date, modeling is still the only possible way to visualize potential structures for most membrane proteins, but those models can subsequently be tested experimentally. In this and the following section we will discuss a model for the transmembrane arrangement of the UCP1 and we will consider the possible location of residues that may be important for nucleotide binding. At present, establishing unequivocally which is the correct arrangement in the membrane is not possible. Our main effort is directed towards the analysis of the structural elements that are important for nucleotide binding and how these elements can be understood in a 3D model. We will now summarize the considerations that we have taken into account to generate the model. The first issue that will be analyzed is the organization of the transmembrane helix bundle.

(a) Sequence analysis of the members of the transporter family reveals the existence of a tripartite structure with three sequence repeats of about 100 amino acids (Aquila *et al*., 1987; Walker and Runswick, 1993) (Fig. 1). Each repeat presents two hydrophobic stretches that very likely constitute α-helical transmembrane segments linked by an extensive hydrophilic loop. Therefore, the complete polypeptide chain is expected to cross the lipid bilayer six times. This transmembrane arrangement has been corroborated for the UCP1 with topological studies performed with antibodies (Miroux *et al*., 1992, 1993) and other members of the carrier family (Bogner *et al*., 1986; Brandolin *et al*., 1989; Hatanaka *et al*., 2001). The N- and C-terminal ends are exposed to the cytosolic side of the membrane and thus the long hydrophilic loops face the matrix side. Fourier-transform infrared spectroscopy has also revealed a high α-helix content and thus agrees with the idea that the TMSs are α-helical (Rial *et al*., 1990).

(b) The six TMSs associate to constitute an antiparallel helix bundle. Each TMS must contain 17–20 amino acids to traverse the 25–30-Å hydrophobic core of the membrane (Winner and White,

1992) although the shortest possible α-helix that can span the core has been shown to be 14 amino acids long (Monne *et al.*, 1999). In the present model, the TMHs have been defined with the help of the MPEx program (Jayasinghe *et al.*, 2001) and they comprise the following residues: Ile^{16}-Leu^{33}, Pro^{78}-Tyr^{95}, Ile^{116}-Thr^{133}, Pro^{178}-Tyr^{194}, Leu^{215}-Val^{232}, and Pro^{272}-Phe^{288}. The beginning of TMH1 and TMH5 cannot be defined unambiguously, and alternatively they could start at Thr^{11} and Val^{211}, respectively. We will however consider the shorter TMHs which present a slightly higher hydrophobic profile and should be long enough to span the hydrophobic core of the membrane.

(c) The helices are grouped sequentially in the barrel. We derive this proposal from the consideration of the biogenesis of membrane proteins and the short length of loops that connect the three repeats. The existence of a lipid bilayer imposes important thermodynamic and geometric constraints on the way in which the bundle can be organized. The current view on the folding of membrane proteins derives from a basic two-stage model where first individual helices of a polytopic protein are formed and are postulated to be stable separately in the lipid bilayer. In a second step, helix–helix interactions lead to the packing of the α-helices (for review see Popot and Engelman, 2000). Arrangements implying crossovers of the loops would complicate the biogenesis and subsequent folding in the membrane (Nelson and Douglas, 1993).

(d) TMSs have an amphiphilic nature and it is expected that the more polar surfaces face the protein interior. Site-directed mutagenesis and selection of second site revertants have been used previously to define the "in–out" orientations for the six transmembrane segments of AAC2 (Nelson and Douglas, 1993). A similar arrangement for the six TMHs of UCP1 can be obtained on the basis of a sequence comparison with AAC2. We have further evaluated these orientations analyzing the profiles of the periodicity in the hydrophobicity and conservation/variability of aligned residues along the length of each predicted TMH, as calculated by PERSCAN v7.0 (Donelly *et al.*, 1993). For the alignment, all available sequences for the UCP1, UCP2, and UCP3 were considered. The in–out orientations agree with the predictions made for AAC2 based on the mutagenesis data (Fig. 4(a)).

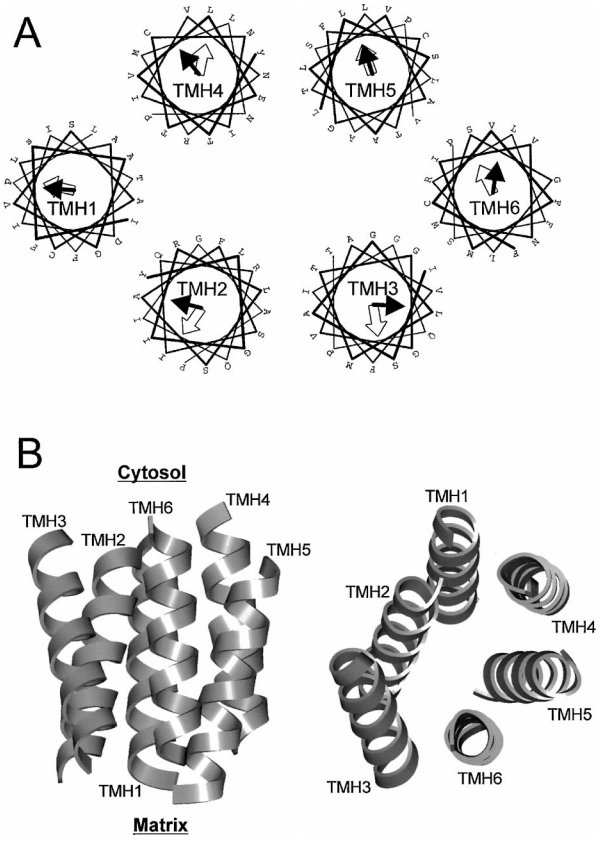

Fig. 4. Model for the transmembrane arrangement of the UCP1. Panel A, helical wheel display of the six transmembrane segments. The hydrophobicity moment for each helix is indicated with a black arrow. The variability moment is indicated with an empty arrow. These two parameters have been calculated by PERSCAN (Donelly *et al.*, 1993) using the available sequences for the UCP1, UCP2, and UCP3. Panel B, in-membrane view (left) and cytosolic view (right) of the 3D model of the helix bundle. See text for further details.

(e) We hypothesize that the hydrophilic interior of the helix bundle constitutes the main translocation pathway (Section 1). Nucleotide binding in UCP1 occurs in the translocation pathway by analogy with the proposal made for the AAC. Intrahelical charged residues that have an influence on binding (Arg^{83}, Arg^{182}, Glu^{190}, and Arg^{276}) face the translocation pathway.

(f) The functional carrier unit is a homodimer (Lin *et al.*, 1980). Experiments performed with the AAC have demonstrated that TMH1 of one monomer and TMH6 of the other must be close to each other because when the two monomers are covalently linked in tandem, the unit is fully functional (Hatanaka *et al.*, 1999; Huang *et al.*, 2001; Trézéguet *et al.*, 2000). The two C-terminal

ends of the UCP1 dimer can be cross-linked, and the dimer retains the nucleotide binding and transport activity (Klingenberg and Appel, 1989).

(g) In the AAC (Huang *et al*., 2001) and the PiC (Schroers *et al*., 1998), the two subunits have been proposed to act interdependently in transport, exhibiting partial cooperativity that would be translated as coordinated conformational rearrangements in the two monomers. Nelson and Douglas have proposed, on the basis of amino acid conservation, that in the AAC the dimer interface would be TMH2–TMH3 (Nelson and Douglas, 1993). Sequence analysis performed with PERSCAN also signifies the presence of highly conserved residues in the hydrophobic face of these two helixes and therefore suggests helix–helix contacts.

The model considers that in each monomer there is a sequential grouping of the TMHs to form the bundle with TMH1, TMH2, and TMH3 in an anticlockwise orientation while TMH4, TMH5, and TMH6 are oriented clockwise (Fig. 4(a)). With this arrangement there is no crossover of the loops. Figure 5 presents a dimer organization. The working hypothesis is based on the existence of one translocation channel in each monomer that is lined with the polar faces of each TMH. The dimer interface is formed by TMH2–TMH3 of each monomer. This organization allows the linkage in tandem of the two subunits proved to be functionally competent (Hatanaka *et al*., 1999; Huang *et al*., 2001; Trézéguet *et al*., 2000).

The next issue concerns the orientation of the long matrix loops with respect to the transmembrane bundle. Two main possibilities are envisaged, either the loops remain outside the bundle or they penetrate, at least partially, into the core. A number of features suggest that the loops constitute the matrix face of the protein.

(h) Topological studies performed with antibodies against short peptides derived from UCP1 revealed that the regions 61–79 (in the 1st matrix loop), 164–184 (in the 2nd matrix loop), and 255–273 (in the 3rd matrix loop) could be recognized from the matrix side of the inner membrane (Miroux *et al*., 1992, 1993). This implies that at least the C-terminal part of these loops must be exposed to the matrix.

(i) If Arg^{83}, Arg^{182}, and Arg^{276} are essential for nucleotide binding it should imply that their side chains must be exposed to the binding pocket. The insertion of the loops into the core of the helix barrel would eclipse these residues.

(j) Our main argument against the penetration of the loops into the barrel core is of sterical nature. If we consider that the average interhelix packing distance in membrane proteins is 9.6 Å (Bowie, 1997), the average diameter of the lumen of the core of an hexagonal arrangement of six α-helices would be $\sim$8 Å. This is insufficient to fit a folded

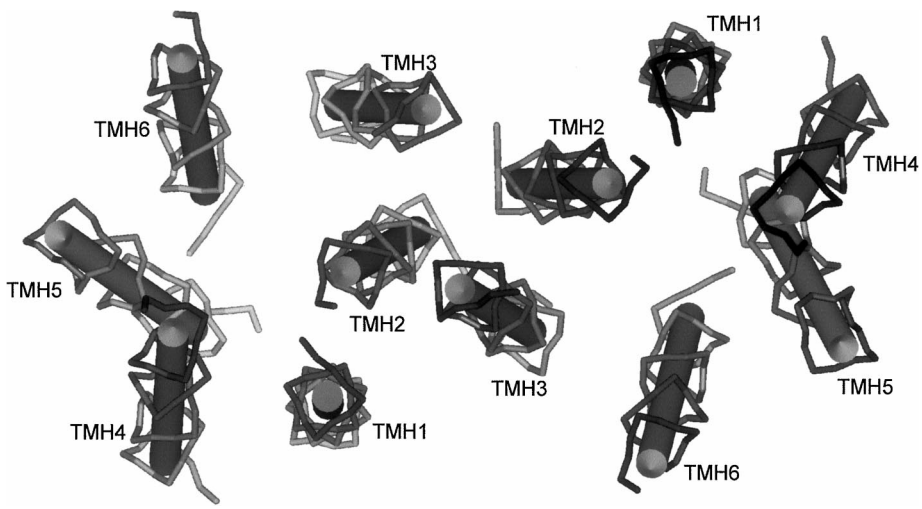

Fig. 5. Model for the arrangement of the UCP1 dimer seen from the cytosolic side of the membrane.

polypeptide chain. As an example of the insertion of a compact structural motif in the core of the bundle, we have measured the average van der Waals thickness of a porin β-hairpin that is $\sim$9 Å. Alternatively, loops could be accommodated increasing the interhelix distance but this would require the loss of helix–helix contacts.

With all these considerations in hand, we have applied computer-aided 3D modeling methods to build a model for the helix bundle of rat UCP1. Six idealized (1.5-Å rise/residue and 3.6 residues/turn) α-helices corresponding to the putative TMH, including the side chains, were constructed with the Insight II computer molecular program (MSI, San Diego, CA). Their N- and C-termini were blocked with acetyl and amide groups, respectively, to mimic the effects of preceding and following peptide bonds within an intact protein.

The helix bundle was assembled analyzing first the interactions on all possible helix pairs by computational docking methods. We used the docking software 3D-Dock (http://www.bmm.icnet.uk/docking), which carries out predictions of protein–protein interactions to perform a conformational search of the packing of all possible helix pairs and the subsequent energy minimization of the side chains on the helix–helix docking interface. The resulting complexes are screened via a constraint "filter" programme. This methodology allowed the identification of a limited set of possible structural associations that were subsequently used to screen for bundles consistent with the knowledge-based restraints and the reported experimental data (see above). The second stage of the model-building procedure was the refinement of the resulting bundle by molecular mechanics energy minimization and restrained molecular dynamics simulations. All calculations were carried out under the AMBER all-atom force field (Weiner *et al*., 1986) on an SGI. Power Challenge R10000 computer. Simulations were performed without any explicit solvent but using a distance-dependent dielectric constant $\varepsilon = R$ (where R is the distance between two interacting atoms) to mimic water's effects on intramolecular interactions. Two classes of restraints were used: (i) an inter-helix distance restraint of $<$9.6 Å (based on the average helix–helix packing distance found in transmembrane proteins (Bowie, 1997)) to prevent the helices from moving too far apart at the beginning of the molecular dynamics run but leaving helices free to rotate around and slide along their respective axes without imposing restraints on the angle between two helices; (ii) an intrahelix donor–acceptor distance restraint $<$3.2 Å for the backbone hydrogen bonds to maintain the α-helicity within each TMH during the simulation (Sansom *et al*., 1998). Energy refinement was done by 500 cycles of steepest-descent minimization followed by 2000 cycles of full-conjugate gradient minimization. Molecular dynamics simulations were performed at 300 K with a step length of 0.001 ps, after an initial equilibrium dynamics phase starting from 0.1 K. The cutoff for the electrostatic interaction was 9.5 Å. The cutoff distance for the nonbonded interaction was 8 Å. Figure 4(b) presents the six-helix bundle that results from the modeling. The helices present roughly a hexagonal grouping and are tilted with respect to the lipid bilayer. The closest interhelix distances range from 7 to 10 Å. Helixes are not parallel and interhelix crossing angles range from -164° to 172° (Chothia *et al*., 1981). The bundle leaves a continuous opening along its center that we propose should correspond to the translocation pore. It presents an average diamater of 4 Å as calculated with HOLE (http://www.bip.bham.ac.uk/hole).

The model for the dimer was built with two identical helix bundles taken as two rigid entities to carry out a 3D-Dock computational search of all optimal interactions between monomers. The results were filtered considering that the dimer interface is formed by TMH2–TMH3 of each monomer (see above).

TOPOLOGY OF THE NUCLEOTIDE-BINDING SITE IN UCP1

The SBCGP model considers the existence of a binding center whose access is controlled by gates. In the previous section we have discussed the evidence suggesting that in the mitochondrial carrier family the most likely configuration is an α-helical bundle formed by the six helices of the monomer and with the hydrophilic translocation path in the center. The two gates would be probably formed by the hydrophilic loops on their respective membrane sides. Purine nucleotides are physiological ligands of two members of the carrier family—the uncoupling proteins and the ADP/ATP carrier—but other members of the family may also be fit to bind nucleotides although this may have no physiological relevance. In fact, it has been shown that the PiC binds nucleotides and inhibits transport (Majima *et al*., 2001; Stappen and Krämer, 1994). We have previously proposed that nucleotides bind to UCP1 deep inside the protein, with the purine ring interacting with the matrix loops (Arechaga *et al*., 2001; González-Barroso *et al*., 1999). Binding studies have demonstrated that only one nucleotide is bound per dimer (Lin and Klingenberg, 1982). However, there must be one nucleotide-binding site in each monomer since at alkaline pH and in the presence of urea, the binding of 1 mol of nucleotide per mol of monomeric UCP1 has been demonstrated (Feil and

Rafael, 1994; Rafael *et al*., 1994). The working hypothesis is that binding to one subunit inhibits binding to the other. We will now try to visualize the nucleotide-binding site in UCP1 taking into account the available nucleotide-binding data and the 3D model presented in the previous section.

Photoaffinity labeling of hamster UCP1 identified the interaction of the purine ring with Cys^{253} and Thr^{264} in the third matrix loop (Mayinger and Klingenberg, 1992; Winkler and Klingenberg, 1992). We have previously reported that Thr^{264} is part of a short α-helix (263–268) at the N-terminal end of TMH6. The connection of the 263–268 α-helix to TMH6 occurs through the sequence Gly-Phe-Val-Pro that could constitute a β-turn of type VIII. Molecular modeling of the connection positions this short α-helix in a plane parallel to the lipid bilayer and in the boundary between the hydrophobic core and the polar region constituted by the head groups of the phospholipids (González-Barroso *et al*., 1999). The interaction of the nucleotide with Thr^{264} helps define the orientation of the 263–268 helix with respect to the hydrophilic interior. If Thr^{264} has to face the core of the bundle, the aromatic rings of Phe^{266} and Phe^{270} would be exposed to the interface between the hydrophobic core and the polar layer of the head groups, this being a common feature in multispanning membrane proteins (Killian and van Heijne, 2000). Since UCP1 binds with high affinity the adenosine and guanosine rings, we propose that stabilization of the ring occurs through stacking interactions rather than the formation of specific hydrogen bonds. Phe^{267} and/or Pro^{263}, on the same side of the 263–368 helix as Thr^{264}, could contribute to the formation of the binding pocket.

The model presented in Fig. 4 suggests that the second matrix loop must consitute a central part in the gating domain. The participation of the loop in the gating had been proposed previously after the observation that His^{145} and His^{147} were essential for H^+ transport in UCP1 (Bienengraeber *et al*., 1998). In this context, we should recall that fluorescence-quenching-resolved spectroscopy demonstrated that the fluorescence of Trp^{173} (located in the second matrix loop in the position equivalent to Phe^{267}) was quenched by iodide and, what is more relevant to the present discussion, nucleotide binding partially shielded Trp^{173} from the interaction with iodide (Viguera *et al*., 1992). Finally, photoaffinity labeling experiments with AAC found nucleotide bound to the second and third matrix loop but not to the first (Dalbon *et al*., 1988; Dianoux *et al*., 2000). It is therefore likely that the binding pocket for the purine moiety in UCP1 is contributed by residues from the second and third matrix loops.

Our proposal for the nucleotide binding to UCP1 (Arechaga *et al*., 2001; González-Barroso *et al*., 1999)

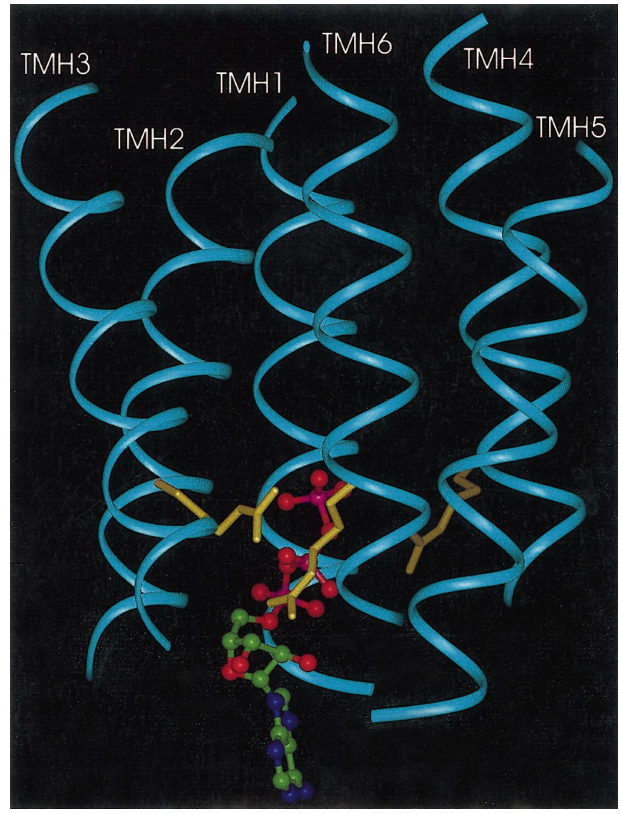

Fig. 6. Model for the position of the nucleotide when bound to UCP1 inside the helix bundle. For clarity, α-helices are shown as ribbons and only Arg^{83}, Arg^{182}, and Arg^{276} are shown to demonstrate the position of the polyphosphate chain with respect to these three residues. See text for further details.

leaves the polyphosphate chain looking up the core of the bundle. Negative charges of the polyphosphate chain could establish salt bridges with any of the Arg residues of TMH2, TMH4, and TMH6 (Arg^{83}, Arg^{182}, and Arg^{276}). Distances from the amino acid side chains to the nucleotide located close to the 263–268 helix (3rd matrix loop) makes possible the interaction with any of these residues. Figure 6 presents an ATP molecule inserted in the bundle in a position compatible with the above considerations. The ATP molecule has been packed into the six-helix bundle using interactive molecular graphics methods. Limited bumping monitor was applied to improve packing and relieve steric clashes introduced during the interactive graphics packing process. The purine ring has been oriented so that the labeling of Thr^{264} is feasible if a reactive group is introduced at position 2 of the ring. The matrix loops cannot be included in the model because their conformation is unknown.

The nucleotide has been fitted in the matrix side of the bundle in a site that we propose should be its final position

in the binding pocket. However, the nucleotide has to reach the binding site from the cytosolic side of the membrane and thus molecular rearrangments should occur during the process. It should be remembered that it has been proposed that binding of the nucleotide occurs in two steps, first a loose binding that it is subsequently converted to tight binding (Huang *et al*., 1998). Glu^{190} and His^{214} have been involved also in the pH dependency of nucleotide binding (Echtay *et al*., 1998; Winkler *et al*., 1997). The 3D model reveals that these residues would be too far from the polyphosphate moiety when the nucleotide is located down inside the binding site. Therefore, Glu^{190} and His^{214} cannot interact with the bound nucleotide. However, since these residues are on the cytosolic side of the barrel, it is very likely that their state of protonation will influence their access to the binding site. The loss of the binding site after modification of Glu^{190} with Woodward reagent K (Winkler *et al*., 1997) could be interpreted as blocking of the access to the binding site.

CONCLUDING REMARKS

In the present review we have attempted to put together all the data available on the binding of nucleotides to the uncoupling protein UCP1 and the adenine nucleotide translocator. As we said earlier, our aim was to understand the structural elements that are important for nucleotide binding by placing these elements on a 3D model. Since several bioinformatic tools allow the modeling of the membrane proteins, biochemical data and molecular modeling have been put together to build a model for the transmembrane section of UCP1 and to position the nucleotide in a location consistent with the available data. The resulting model is hypothetical. Nevertheless, it is a starting point to understand how the uncoupling protein UCP1 is regulated and how it may be interacting with the nucleotide. Biochemical tests and high resolution structural data will determine the validity of this exercise.

ACKNOWLEDGMENTS

This work has been supported by a grant from the Spanish Ministry of Science and Technology (BIO99-0870). AL is supported by a grant from the Comunidad de Madrid.

REFERENCES

Abrahams, J. P., Leslie, A. G. W., Lutter, R., and Walker, J. E. (1994). *Nature* **370**, 621–628.

Anderson, P. A. V., and Greenberg, R. M. (2001). *Comp. Biochem. Physiol. B* **129**, 17–28.

Aquila, H., Link, T. A., and Klingenberg, M. (1987). *FEBS Lett.* **212**, 1–9.

Arechaga, I., Ledesma, A., and Rial, E. (2001). *IUBMB Life* **52**, 165–173.

Berry, M. B., Meador, B., Bilderback, T., Liang, P., Glasser, M., and Phillips, G. N., Jr. (1994). *Proteins: Struct., Funct., Genet.* **19**, 183–198.

Bienengraeber, M., Echtay, K. S., and Klingenberg, M. (1998). *Biochemistry* **37**, 3–8.

Bogner, W., Aquila, H., and Klingenberg, M. (1986). *Eur. J. Biochem.* **161**, 611–620.

Boss, O., Hagen, T., and Lowell, B. B. (2000). *Diabetes* **49**, 143–156.

Bowie, J. U. (1997). *J. Mol. Biol.* **272**, 780–789.

Brandolin, G., Boulay, F., Dalbon, P., and Vignais, P. V. (1989). *Biochemistry* **28**, 1093–1100.

Brown, G. C., Nicholls, D. G., and Cooper, C. E. (Eds.). (1999). Biochem. Soc. Symp. **66**. Portland Press, London.

Brustovetsky, N., and Klingenberg, M. (1996). *Biochemistry* **35**, 8483–8488.

Cammack, J. N., and Schwartz, E. A. (1996). *Proc. Natl. Acad. Sci. U.S.A.* **93**, 723–727.

Costantini, P., Belzacq, A. S., Vieira, H. L. A., Larochette, N., de Pablo, M. A., Zamzami, N., Susin, S. A., Brenner, C., and Kroemer, G. (2000). *Oncogene* **19**, 307–314.

Chothia, C., Levitt, M., and Richardson, D. (1981). *J. Mol. Biol.* **145**, 215–250.

Crompton, M., Ellinger, H., and Costi, A. (1988). *Biochem. J.* **255**, 357–360.

Dalbon, P., Brandolin, G., Boulay, F., Hoppe, J., and Vignais, P. V. (1988). *Biochemistry* **27**, 5141–5149.

Dianoux, A. C., Noël, F., Fiore, C., Trézéguet, V., Kieffer, S., Jaquinod, M., Lauquin, G. J. M., and Brandolin, G. (2000). *Biochemistry* **39**, 11477–11487.

Dierks, T., Salentin, A., and Krämer, R. (1990). *Biochim. Biophys. Acta* **1028**, 281–288.

Dierks, T., Stappen, R., and Krämer, R. (1994). In *Molecular Biology of Mitochondrial Transport Systems* (Forte, M., and Colombini, M., eds.) , Springer-Verlag, Berlin, pp. 117–129.

Donelly, D., Overington, J. P., Ruffle, S. V., Nugent, J. H., and Blundell, T. L. (1993). *Protein Sci.* **2**, 55–70.

Echtay, K. S., Bienengraeber, M., and Klingenberg, M. (2001). *Biochemistry* **40**, 5243–5248.

Echtay, K. S., Bienengraeber, M., Winkler, E., and Klingenberg, M. (1998). *J. Biol. Chem.* **273**, 24368–24374.

Echtay, K.S., Winkler, E., Bienengraeber, M., and Klingenberg, M. (2000). *Biochemistry* **39**, 3311–3317.

Feil, S., and Rafael, J., (1994). *Eur. J. Biochem.* **219**, 681–690.

Fry, D. C., Kuby, S. A., and Mildvan, A. S. (1986). *Proc. Natl. Acad. Sci. U.S.A.* **83**, 907–911.

González–Barroso, M. M., Fleury, C., Jiménez, M. A., Sanz, J. M., Romero, A., Bouillaud, F., and Rial, E. (1999). *J. Mol. Biol.* **292**, 137–149.

González-Barroso, M. M., Fleury, C., Levi-Meyrueis, C., Zaragoza, P., Bouillaud, F., and Rial, E. (1997). *Biochemistry* **36**, 10930–10935.

Hagen, T., Zhang, C., Vianna, C. R., and Lowell, B. B. (2000). *Biochemistry* **39**, 5845–5851.

Halestrap, A. P., and Davidson, A. M. (1990). *Biochem. J.* **268**, 153–160.

Halestrap, A. P., McStay, G. P., and Clarke, S. J. (2002). *Biochimie* **84**, 153–166.

Halestrap, A. P., Woodfield, K. Y., and Connern, C. P. (1997). *J. Biol. Chem.* **272**, 3346–3354.

Hashimoto, M., Majima, E., Goto, S., Shinohara,Y., and Terada, H. (1999). *Biochemistry* **38**, 1050–1056.

Hatanaka, T., Hashimoto, M., Majima, E., Shinohara, Y., and Terada, H. (1999). *Biochem Biophys Res. Commun.* **262**, 726–730.

Hatanaka, T., Kihira, Y., Shinohara, Y., Majima, E., and Terada, H. (2001). *Biochem. Biophys. Res. Commun.* **286**, 936–942.

Heaton, G. M., and Nicholls, D. G. (1977). *Biochem. Soc. Trans.* **5**, 210–212.
Heaton, G. M., Wagenvoord, R. J., Kemp, A., and Nicholls, D. G. (1978). *Eur. J. Biochem.* **82**,515–521.
Heidkämper, D., Müller, V., Nelson, D. R., and Klingenberg, M. (1996). *Biochemistry* **35**, 16144–16152.
Herick, K., Krämer, R., and Lühring, H. (1997). *Biochim. Biophys. Acta* **1321**, 207–220.
Hernández, J. A. (2001). *J. Membr. Biol.* **180**, 177–185.
Huang, S. G., and Klingenberg, M. (1995). *Biochemistry* **34**, 349–360.
Huang, S. G., and Klingenberg, M. (1996). *Biochemistry* **35**, 16806–16814.
Huang, S. G., Lin, Q. S., and Klingenberg, M. (1998). *J. Biol. Chem.* **273**, 859–864.
Huang, S. G., Odoy, S., and Klingenberg, M. (2001). *Arch. Biochem. Biophys.* **394**, 67–75.
Huber, T., Klingenberg, M., and Beyer, K. (1999). *Biochemistry* **38**, 762–769.
Indivieri, C., Tonazzi, A., Dierks, T., Krämer, R., and Palmieri, F. (1992). *Biochim. Biophys. Acta* **1140,** 53–58.
Jaburek, M., Varecha, M., Gimeno, R. E., Dembski, M., Jezek, P., Zhang, M., Burn, P., Tartaglia, L. A., and Garlid, K. D. (1999). *J. Biol. Chem.* **274**, 26003–26007.
Jayasinghe, S., Hristova, K., and White, S. H. (2001). *J. Mol. Biol.* **312**, 927–934.
Kabsch, W., Mannherz, H. G., Suck, D., Pai, E. F., and Holmes, K. C. (1990). *Nature* **347**, 37–44.
Killian, J. A., and van Heijne, G. (2000). *Trends Biochem. Sci.* **25**, 429–434.
Klingenberg, M. (1988). *Biochemistry* **27**, 781–791.
Klingenberg, M. (1991). *A Study of Enzymes: Mechanism of Enzyme Action* (Kuby, S. A., ed.), CRC Press, Boca Raton, pp. 367–390.
Klingenberg, M., and Appel, M. (1989). *Eur. J. Biochem.* **180**, 123–131.
Klingenberg, M., and Echtay, K. S. (2001). *Biochim. Biophys. Acta* **1504**, 128–143.
Klingenberg, M., Mayer, I., and Dahms, A. S. (1984). *Biochemistry* **23**, 2442–2449.
Krämer, R. (1994). *Biochim. Biophys. Acta* **1185**, 1–34.
Läuger, P. (1987). *Physiol. Rev.* **67**, 1296–1331.
Lin, C. S., Hackenberg, H., and Klingenberg, M. (1980). *FEBS Lett.* **113**, 304–306.
Lin, C. S., and Klingenberg, M. (1982). *Biochemistry* **21**, 2950–2956.
Majima, E., Ikawa, K., Takeda, M., Hashimoto, M., Shinohara, Y., and Terada, H. (1995). *J. Biol. Chem.* **270**, 29548–29554.
Majima, E., Ishida, M., Miki, S., Shinohara, Y., and Terada, H. (2001). *J. Biol. Chem.* **276**, 9792–9799.
Majima, E., Koike, H., Hong, Y. M., Shinohara, Y., and Terada, H. (1993). *J. Biol. Chem.***268**, 22181–22187.
Majima, E., Shinohara, Y., Yamaguchi, N., Hong, Y. M., and Terada, H. (1994). *Biochemistry* **33**, 9530–9536.
Majima, E., Yamaguchi, N., Chuman, H., Shinohara, Y., Ishida, M., Goto, S., and Terada, H. (1998). *Biochemistry* **37**, 424–432.
Mayinger, P., and Klingenberg, M. (1992). *Biochemistry* **31**, 10536–10543.
Mayinger, P., Winkler, E., and Klingenberg, M. (1989). *FEBS Lett.* **244**, 421–426.
Menz, R. I., Walker, J. E., and Leslie, A. G. W. (2001). *Cell* **106**, 331–341.
Miroux, B., Casteilla, L., Klaus, S., Raimbault, S., Grandin, S., Clément, J. M., Ricquier, D., and Bouillaud, F. (1992). *J. Biol. Chem.* **267**, 13603–13609.
Miroux, B., Frossard, V., Raimbault, S., Ricquier, D., and Bouillaud, F. (1993). *EMBO J.* **12**, 3739–3745.
Modriansky, M., Murdza–Inglis, D., Patel, H. V., Freeman, K. B., and Garlid, K. D. (1997). *J. Biol. Chem.* **272**, 24759–24762.
Monne, M., Nilsson, I., Elofsonn, A., and von Heijne, G. (1999). *J. Mol. Biol.* **293**, 807–814.
Müller, V., Basset, G., Nelson, D. R., and Klingenberg, M. (1996). *Biochemistry* **35**, 16132–16143.
Nelson, D. R., and Douglas, M. G. (1993). *J. Mol. Biol.* **230**, 1171–1182.
Nelson, D. R., Felix, C. N., and Swanson, J. M. (1998). *J. Mol. Biol.* **277**, 285–308.
Nelson, D. R., Lawson, J. E., Klingenberg, M., and Douglas, M. (1993). *J. Mol. Biol.* **230**, 1159–1170.
Nicholls, D. G. (1976). *Eur. J. Biochem.* **63**, 223–228.
Nicholls, D. G., and Locke, R. M. (1984). *Physiol. Rev.* **64**, 1–64.
Popot, J. L., and Engelman, D. M. (2000). *Annu. Rev. Biochem.* **69**, 881–892.
Quick, M., Loo, D. D. F., and Wright, E. M. (2001). *J. Biol. Chem.* **276**, 1728–1734.
Rafael, J., Pampel, X., and Wang, X. (1994). *Eur. J. Biochem*. **223**, 971–980.
Rial, E., and González-Barroso, M. M. (2001). *Biochim. Biophys. Acta* **1504**, 70–81.
Rial, E., González-Barroso, M. M., Fleury, C., Iturrizaga, S., Sanchis, D., Jiménez-Jiménez, J., Ricquier, D., Goubern, M., and Bouillaud, F. (1999). *EMBO J.* **18**, 5827–5833.
Rial, E., Muga, A., Valpuesta, J. M., Arrondo, J. L. R., and Goñi, F. M. (1990). *Eur. J. Biochem.* **188**, 83–89.
Rial, E., and Nicholls, D. G. (1986). *Eur. J. Biochem.* **161**, 689–692.
Ricquier, D., and Bouillaud, F. (2000). *Biochem. J.* **345**, 161–179.
Ross, P. D., and Subramanian, S. (1981). *Biochemistry* **20**, 3096–3102.
Rossman, M. G., Liljas, A., Brändén, C. I., and Banaszak, L. J. (1975). *Enzymes* **11**, 61–102.
Sack, S., Kull, F. J., and Mandelkow, E. (1999). *Eur. J. Biochem.* **262**, 1–11.
Saier, M. H., Jr. (2000a). *Microbiol. Mol. Biol. Rev.* **64**, 354–411.
Saier, M. H., Jr. (2000b). *J. Bacteriol.* **182**, 5029–5035.
Sansom, M. S. P., Kerr, I. D., Law, R., Davison, L., and Tieleman, D. P. (1998). *Biochem. Soc. Trans.* **26**, 509–515.
Schroers, A., Burkovsky, A., Wohlrab, H., and Krämer, R. (1998). *J. Biol. Chem.* **273**, 14269–14276.
Schwarz, M., Gross, A., Steinkamp, T., Flügge, U. I, and Wagner, R. (1994). *J. Biol. Chem.* **269**, 29481–29489.
Simon, I., Fiser, A., and Tusnády, G. A. (2001). *Biochim. Biophys. Acta* **1549**, 123–136.
Sprang, S. R. (1997). *Annu. Rev. Biochem.* **66**, 639–678.
Stappen, R., and Krämer, R. (1993). *Biochim. Biophys. Acta* **1149**, 40–48.
Stappen, R., and Krämer, R. (1994). *J. Biol. Chem.* **269,** 11240–11246.
Stuart, J. A., Cadenas, S., Jekabsons, M. B., Roussel, D., and Brand, M. D. (2001). *Biochim. Biophys. Acta* **1504**, 144–158.
Trézéguet, V., Le Saux, A., David, C., Gourdet, C., Fiore, C., Dianoux, A. C., Brandolin, G., and Lauquin, G. (2000). *Biochim. Biophys. Acta* **1457**, 81–93.
Viguera, A. R., Goñi, F. M., and Rial, E. (1992). *Eur. J. Biochem.* **210**, 893–899.
Walker, J. E. and Runswick, M. J. (1993). *J. Bioenerg. Biomembr.* **25**, 435–446.
Walker, J. E., Saraste, M., Runswick, M. J., and Gay, N. J. (1982). *EMBO J.* **8**, 945–951.
Weiner, S. J., Kollman, P. A., Nguyen, D. T., and Case, D. A. (1986). *J. Comp. Chem.* **7**, 230–252.
Winkler, E., and Klingenberg, M. (1992). *Eur. J. Biochem.* **203**, 295–304.
Winkler, E., Wachter, E., and Klingenberg, M. (1997). *Biochemistry* **36**, 148–155.
Winner, M. C., and White, S. H. (1992). *Biophys. J.* **61**, 437–447.